TECHNICAL NOTE

D-1304

SECONDARY FLOW FIELDS EMBEDDED IN

HYPERSONIC SHOCK LAYERS

By Alvin Seiff

Ames Research Center
Moffett Field, Calif.

NATIONAL AERONAUTICS AND SPACE ADMINISTRATION

WASHINGTON   May 1962

L

NATIONAL AERONAUTICS AND SPACE ADMINISTRATION

TECHNICAL NOTE D-1304

SECONDARY FLOW FIELDS EMBEDDED IN

HYPERSONIC SHOCK LAYERS

By Alvin Seiff

SUMMARY

When a ramp or other compression surface is located in a locally supersonic region behind a hypersonic bow shock wave, it generates a secondary shock wave. The ramp flow disturbance may be viewed as an embedded Newtonian impact flow if the embedded shock layer is thin. Examination of the applicability of Newtonian flow theory to cones and wedges in uniform streams suggests that this theory can be expected to give a useful approximation to the surface pressures.

A pressure equation based on this concept predicts a number of interesting things: First, pressures can differ from simple Newtonian theory by factors of 1/5 to 3; for example, on flare stabilizers on blunt-nosed bodies of revolution, pressures are lower than Newtonian and diminish with increasing flight speed in the hypersonic speed range. The calculated pressures vary over the flare surface as a result of the nonuniformity of its incident stream, and depend on the axial location of the flare. In the case of a flap mounted on a large-angled blunt-nosed cone, the pressure coefficients vary from 1 to 5 through the variable entropy layer. A pressure coefficient of 5 greater than the maximum possible in Newtonian flow can occur because the compression process is more efficient than a single shock wave process. On areas of the flap that protrude through the main bow wave, the pressure coefficient should revert to the simple Newtonian value.

Equations are developed for the initial slopes of the normal-force and pitching-moment curves of a flare stabilizer. In the simplest case these differ from conventional Newtonian theory by the ratio of local dynamic pressure to free-stream dynamic pressure. This ratio takes values as low as 0.1 in some of the examples considered.

INTRODUCTION

A compression corner on the surface of a body in hypersonic flight will generate an oblique shock wave if it is located in a locally supersonic region. This kind of flow configuration occurs on flare-stabilized bodies and on bodies with flap controls, for example. Newtonian theory,

which stipulates that there be a bow shock wave closely wrapped around the body, fails to provide the secondary shock wave. As such, it may be appreciably in error even in the hypersonic limit.

For attached flow, two-dimensional flow theory may be used to obtain pressures on the ramp at the corner, provided the conditions upstream of the corner are known. Away from the corner, no simple theory exists for calculating the pressure distribution. Strongly nonuniform stream conditions at the station of the ramp complicate the problem. In reference 1, a simple theory appropriate to these conditions, referred to as embedded Newtonian flow theory, was proposed for the case of flare stabilizers. The purpose of the present note is to develop this concept further, to investigate the conditions for which it should be valid, and to show some predicted consequences in contrasting examples. Comparisons with conventional Newtonian impact theory are included. Equations for the initial normal-force and pitching-moment curve slopes of a flare stabilizer are derived.

SYMBOLS

C_m pitching moment based on cylinder area and cylinder radius

$C_{m_{\alpha_1}}$ initial slope of pitching-moment curve

C_N normal-force coefficient based on cylinder area

$C_{N_{\alpha_1}}$ initial slope of normal-force curve

C_p pressure coefficient, $\dfrac{p - p_\infty}{q_\infty}$

d   cylinder diameter

l_f flare length

M   Mach number

n   coordinate normal to cone surface

p   static air pressure

q   dynamic pressure, $\dfrac{\rho u^2}{2}$

r   radius normal to body axis of symmetry

r_n nose radius of curvature

T   temperature

u	air velocity
x	axial distance from stagnation point
α	angle of attack
γ	ratio of specific heats
θ	cone or ramp half-angle
ξ	angle between streamline and surface normal
ρ	air density
φ	azimuth angle
X	distance from leading edge of flare to its center of pressure

Subscripts

1	properties in region 1 ahead of ramp shock wave
2	properties in region 2 behind ramp shock wave
∞	free stream
b	base
c	cylinder
le	leading edge
s	bow shock wave

A
5
4
1

EMBEDDED NEWTONIAN FLOWS

Two flow configurations of the kind under consideration are shown
in sketches (a) and (b). In both cases, compression corners occur in
locally supersonic regions of hypersonic flow fields, and generate
secondary shock waves. Note also that the closely wrapped bow shock wave
assumed in Newtonian theory is not realized for cases like that in sketch
(a), according to information given in reference 2.

Sketch (a)   Sketch (b)

Assuming for the moment that the embedded shock layers (regions 2) are
thin, as shown, it seems natural to consider treating the ramp by an
impact flow model, with conditions along the surface of the secondary
shock wave as initial conditions. The validity of the results obtained
would then depend on (1) the thickness of the secondary shock layer, and
(2) the occurrence of attached, as opposed to separated, flow in the
corner. The former point will be treated in some detail in the next
section. The latter point cannot be quantitatively discussed at the
present state of knowledge. However, it is known empirically that a wide
range of ramp angles and Reynolds numbers will support attached flow or
flow which is only locally separated in the vicinity of the corner. For
large ramp angles, or ramp heights which are large compared to other body
dimensions, separated flow will occur. For example, a 90° ramp will
invariably separate the flow. The embedded Newtonian flow concept could,
in principle, be applied to these cases also, provided the separated flow
boundary can be described.

Methods are available for calculating the properties of the streams
which are incident on the embedded ramps. For example, cases like that
in sketch (a) can be treated by the methods described in reference 3, and
cases similar to that in sketch (b) can be analyzed by the stream tube
method of reference 4. Other procedures are known, as well, by which
these incident conditions can be calculated.

Thickness of the Shock Layer

The limitation to a thin shock layer will now be examined from previously existing information on simple cones and wedges in uniform streams. The Newtonian theory for pressures and forces on pointed cones is very successful, as shown in figure 1, where it is compared with the results of conical flow theory for ideal air taken from reference 5. The latter is exact for the surface pressures at zero angle of attack, but makes use of a linearized perturbation of the zero angle pressures to obtain $C_{N_{\alpha_i}}$. The accuracy given by the impact theory would certainly be considered satisfactory for most purposes. The thickness angles of the shock-layer range from 1° to 8° for the ideal gas flow at infinite Mach number, and from 10° to 15° for the flow Mach number of 3. These shock layers may be said to be thin for purposes of the impact theory.

The Newtonian theory for two-dimensional wedge flow, representative of conditions immediately behind the compression corner, is shown in figure 2. The errors are larger than in the case of cone flow. The shock-layer thickness angles range from 0° to 16° at infinite Mach number and from 17° to 22° at $M_\infty = 3$. Reasonably accurate predictions occur at thickness angles below about 15°.

It will be noted that the Mach numbers approaching the ramp in cases of present interest will not ordinarily exceed 3, even for very high values of the free-stream Mach number. Curves for this Mach number were therefore included in figures 1 and 2. However, the ideal gas theories with $\gamma = 1.4$ are not appropriate for hypersonic free flight. It is interesting that ramp flows like those shown in sketches (a) and (b) differ from usually considered real gas flows in that the stream approaching the ramp is of high static temperature. Solutions, such as those given in reference 6, for two-dimensional oblique shock waves in real gas are for free-stream temperatures near room temperature. Some examples of two-dimensional real-gas ramp flows were calculated for stream conditions similar to that in sketch (a) to see how the results would compare with those of reference 6 and those of figure 2(b). The ramp leading edge was taken to be 2.7 diameters behind the nose of a blunt-nosed cylinder for a free-stream speed of 20,000 ft/sec at an altitude of 175,000 feet. This example is considered in reference 3 and the local flow velocity, Mach number, and static temperature in the stream approaching the ramp are 13,400 ft/sec, 3.04, and 7840° R, respectively. The results compare with the ideal-gas solution and the cold stream real-gas solution in the following way:

Ramp angle	Shock-wave angle			Density ratio across wave		
	This case	Ideal gas	Ref. 6	This case	Ideal gas	Ref. 6
10°	23.6°	27.1°	---	1.80	1.66	3.8
30°	43.3°	52.5°	35.8°	3.98	3.22	6.8

The results from reference 6 are for the given velocity incident on the ramp, 13,400 ft/sec, and the ideal-gas values are for the given incident Mach number, 3.04. The embedded ramp flow lies between these two. The shock layer is thinner than for the ideal-gas curves; hence, as would be expected, slightly improved agreement of the surface pressure coefficient with impact theory is shown in figure 2(a) by the circular symbols. Excellent agreement with impact theory is shown by the real gas in a cold stream, square symbol in figure 2(a).

The above considerations, particularly figure 1, show that the shock layers in embedded ramp flows are, for wide ranges of conditions, thin enough that a Newtonian approximation is useful. One final point should be made. The shock angle tends to diminish with distance away from the compression corner because of two factors: (1) the flow is initially two-dimensional and then approaches conical flow, and (2) the static temperature in the incident stream decreases with increasing radial distance from the axis of symmetry (ref. 3). The latter acts to make the oblique shock wave agree more closely with the solution for a cold free stream. If the shock-layer angle is initially small enough to justify the Newtonian approximation, it will therefore remain small enough and become smaller. Equally important, if the angle is initially in the marginal range for impact theory (15° to 20°), it can come into the accurate range away from the corner so that the impact theory may again yield useful results.

Pressure Equation

The pressure equation for embedded Newtonian flow is simple in form, and leads to an insight into the characteristics of embedded ramp flows. Following the usual line of development for the Newtonian pressure relation, but using the conditions 1 along the front surface of the ramp shock wave as initial conditions, we write

$$p_2 - p_1 = \rho_1 (u_1 \sin \theta)^2 \tag{1}$$

thus expressing the condition that pressure in the shock layer must be that required to bring the momentum normal to the body surface to zero in region 2. This relation can be rewritten in terms of pressure coefficients based on free-stream static and dynamic pressure to obtain

$$C_{p_2} = \frac{p_2 - p_\infty}{q_\infty} = C_{p_1} + 2 \frac{q_1}{q_\infty} \sin^2 \theta \tag{2}$$

or

$$C_{p_2} = C_{p_1} + \frac{q_1}{q_\infty} C_{p_{2\text{Newtonian}}} \qquad (2a)$$

where $C_{p_{2\text{Newtonian}}}$ is the pressure coefficient given for this surface by usual Newtonian impact theory.

Equation (2) is reminiscent of equations used for estimating tail effectiveness in airplane design. The tail force is analyzed by considering the local flow conditions, principally speed and downwash angle. Similarly, in equation (2), the local dynamic pressure, q_1, and local static-pressure coefficient, C_{p_1}, determine the pressure on the ramp.

As noted earlier, the stream approaching the embedded ramp is generally nonuniform. On pointed bodies this may be due simply to variations in the static-pressure field, but with blunt-nosed bodies at hypersonic speeds, it is largely due to curvature of the bow shock wave, and the resulting gradients of entropy and total pressure in a direction normal to the streamlines. The effect of the nonuniform stream on the ramp is predicted by equation (2) when the variation in the incident stream properties is inserted. As long as the shock layer remains thin, the predicted variation should be valid. In examples studied by the author, the pressure tends to rise with increasing distance along the ramp, since q_1 is minimum in the low energy air which passed through the strong shock wave near the body axis.

RESULTS OF APPLYING EQUATION (2) TO TYPICAL PROBLEMS

The results of applying equation (2) to the flow problems illustrated in sketches (a) and (b) will now be presented. These two applications differ in the level of density in the air approaching the ramp; in sketch (a), it is below free-stream density, and in sketch (b), well above free-stream density. This difference has a pronounced effect on the incident dynamic pressure.

Ramp or Flare on a Cylindrical Body With a Blunt Nose

From reference 3, conditions in region 1 of sketch (a) for the station 2.7 diameters back on a hemisphere cylinder at a flight speed of 20,000 ft/sec and 175,000 feet altitude are $C_{p_1} = 0.023$ ($p_1/p_\infty = 6.4$), $q_1/q_\infty = 0.13$. Theoretical pressure coefficients at the beginning of flares originating at this station are:

Flare angle	Pressure coefficient from-	
	Equation (2)	Newtonian theory
10°	0.031	0.0604
20°	.053	.234
30°	.087	.500

These pressures are plotted against flare angle in figure 3.

Calculations of q_1/q_{∞} and C_{p_1} show a dependence on flight speed, for a given location on the body, as is seen in the example in figure 4. These values were calculated for real-gas flow at equilibrium by the machine program method of reference 3. The dynamic-pressure ratio decreases steadily with increasing flight speed. (As noted in reference 1, a reduction in dynamic-pressure ratio is also given by less exact calculations for an ideal gas, and is attributable to increasing strength of the bow shock wave with increasing flight speed.) The predicted variation with flight speed of pressure coefficient at a flare leading edge is shown in figure 5. Contrary to any expectations of a hypersonic "freeze" of static-pressure coefficients on the flare, the pressure coefficients are seen to vary significantly with increasing speed over the entire range considered, although the variation flattens out at the higher speeds.

Equation (2) further predicts an effect on flare pressure coefficient of location of the flare along the body. The static pressure along the cylinder diminishes with increasing distance from the nose. (This is predicted by blast-wave theory and is borne out by more exact theories.) As a consequence, both C_{p_1} and q_1 decrease with increasing distance from the nose, the latter through the effect of static pressure on air density. The magnitude of these effects on flare leading-edge pressure is shown in figure 6. The static-pressure coefficient changes by more than a factor of 2 in all cases as the flare is moved rearward.

The effect of stream nonuniformity is shown in figure 7. Variations with axial position and radial position, both effective in determining conditions along the flare shock front, act in opposite directions - the dynamic pressure tends to increase with increasing radial distance from the axis and to decrease with increasing axial distance from the nose. Furthermore, the stream static-pressure coefficient, C_{p_1}, decreases with increasing axial distance from the nose. The net effect for flares with base diameters equal to twice the body cylinder diameter depends on flare angle (see fig. 7). On the 10° flare, the predicted surface pressure is nearly uniform, showing about a 10-percent decrease from the leading edge to the base. This results from a nearly perfect cancellation of the opposing effects of position on the static and dynamic pressures ahead of the flare shock wave. In the cases of the larger flare angles, the static-pressure term becomes small compared to the dynamic-pressure term - the latter predominates. Also, on the large angled flares, larger dynamic-pressure variations occur, because of the short length of the flare.

With the 30° flare, the surface static-pressure coefficient is predicted to increase by a factor of 3 from the leading edge to the base.

In brief, these predictions show marked disagreement with simple Newtonian theory for the static pressure on the flares, important effects of flight speed in the high-speed range, important effects of axial location of the flare, and significant variations in pressure over the surface of the flare.

Control Flap on a Round-Nosed Cone

Turning now from the type of body and flow configuration shown in sketch (a) to those in sketch (b), the essential difference as noted is the higher air density in the shock layer ahead of the flap. The flow velocities, except for the region of the spherical nose and the high-entropy layer near the surface, are only slightly reduced from free-stream values, being approximately given by the Newtonian expression, $u_1 = u_\infty \cos \theta$. In figure 8, the results of some unpublished calculations of the shock-layer flow distributions made by the author for a 30° half-angle round-nosed cone are given for two conditions, ideal-gas flow at a Mach number of 10, and real-gas flow at a speed of 33,000 ft/sec at an altitude of 171,500 ft ($M = 29.8$). These distributions show large gradients through the variable entropy layer. In the outer region, the density and velocity come to relatively constant values which are near those that would be obtained with a pointed cone at the same flight conditions. The dynamic pressure parallel to the conical surface undergoes a sizable variation with distance from the surface, but is generally higher than in the free stream, up to a maximum of nine times free-stream dynamic pressure in these examples. The Mach numbers in the shock layer near the cone base range from 1.56 at the body surface to 5.71 at the shock wave for the $M = 29.8$ flight condition. Corresponding values for the ideal gas at a flow Mach number of 10 are 1.45 and 3.26. Therefore, a deflected flap in the shock layer will generate a secondary shock wave.

The result of applying equation (2) to these conditions is shown in figure 9 for a flap deflected 30° relative to the cone surface. Pressure coefficient varies strongly through the variable entropy layer, and reaches values well in excess of 2, the maximum possible pressure coefficient according to Newtonian theory. This implies merely that a more efficient pressure recovery process than those considered by Newtonian theory has been employed. The efficiency of pressure recovery is still fantastically small compared to that which could be obtained by isentropic compression of the gas in the free stream. By comparison of the curves for the two speed conditions, a sensitivity to speed is indicated which is again far from negligible.

If the flap chord is long enough, it will project through the bow shock wave of the parent body. At 33,000 ft/sec with the example geometry, this will occur with 30° flap deflection when the flap chord is longer

than about 5 percent of the body diameter. The portion of the flap outboard of the main bow wave is expected to revert to a single shock wave flow configuration, for which simple Newtonian theory applies. The pressure coefficient should therefore drop to the Newtonian value in the outboard region of a long flap. The chordwise pressure distribution on the flap at $M = 29.8$ would then be rather complicated, beginning at a pressure coefficient less than 1, climbing to a plateau value of about 5, and, near the trailing edge, dropping below 2. It should again be noted that these considerations are restricted to attached flows. In the event of extensive separation, still more complicated variations than those described may occur.

NORMAL FORCE AND PITCHING MOMENT OF A FLARE AT SMALL ANGLE OF ATTACK

On the basis of equation (2), which gives the pressure coefficients on a flare at zero angle of attack, an extension to the case of a small angle of attack can be made to obtain the initial slopes of the normal-force and pitching-moment curves. In terms of the angle ξ between the local stream direction ahead of the flare shock wave and a normal to the flare surface,

$$C_{p_2} = C_{p_1} + 2 \frac{q_1}{q_\infty} \cos^2 \xi \tag{3}$$

where ξ is a function of the angle of attack, α_1, the flare half-angle, θ, and the azimuthal angle, φ,

$$\cos \xi = \cos \alpha_1 \sin \theta + \sin \alpha_1 \cos \theta \cos \varphi \tag{4}$$

The angle of attack α_1 is the projection on the plane of symmetry of the angle between the local stream direction ahead of the flare shock wave and the body axis. In the nonuniform stream ahead of the flare, it should be considered a variable along with C_{p_1} and q_1.

Integration of the elementary pressure forces around φ and along the length of the flare gives the normal-force equation,

$$C_N = \frac{2}{\pi \tan \theta} \int_1^{r_b/r_c} \left(\int_0^\pi C_{p_2} \cos \varphi \, d\varphi \right) \frac{r}{r_c} \, d \frac{r}{r_c} \tag{5}$$

On substitution of equations (3) and (4) into (5), the integral around φ becomes

$$\int_0^\pi C_{p_2} \cos \varphi \, d\varphi = 2 \sin^2\theta \int_0^\pi \frac{q_1}{q_\infty} \cos^2\alpha_1 \cos \varphi \, d\varphi$$

$$+ \sin 2\theta \int_0^\pi \frac{q_1}{q_\infty} \sin 2\alpha_1 \cos^2\varphi \, d\varphi$$

$$+ 2 \cos^2\theta \int_0^\pi \frac{q_1}{q_\infty} \sin^2\alpha_1 \cos^3\varphi \, d\varphi$$

$$+ \int_0^\pi C_{p_1} \cos \varphi \, d\varphi \tag{6}$$

Equation (6) cannot be integrated unless the distributions of α_1, q_1, and C_{p_1} are known and expressible in closed form. Since this implies a more complete knowledge of the flow field in region 1 at angle of attack than is available, the following assumptions are introduced:

1. Assume C_{p_1} independent of φ.

2. Assume $\alpha_1 = \alpha_\infty$.

3. Assume q_1 independent of φ.

Errors due to assumptions (1) and (2) are to some extent self-compensating (as may be seen from their effect on eq. (3)) and in any case should be small at small angles of attack. With one additional assumption, q_1 independent of r, equation (5) may be integrated in closed form to obtain

$$C_N = \frac{q_1}{q_\infty} \left[\left(\frac{r_b}{r_c}\right)^2 - 1 \right] \sin 2\alpha_\infty \cos^2\theta = \frac{q_1}{q_\infty} C_{N_{\text{Newtonian}}} \tag{7}$$

which is limited to small angles of attack. Differentiation to obtain the initial slope yields

$$C_{N_{\alpha_i}} = 2 \frac{q_1}{q_\infty} \left[\left(\frac{r_b}{r_c}\right)^2 - 1 \right] \cos^2\theta = \frac{q_1}{q_\infty} \left(C_{N_{\alpha_i}} \right)_{\text{Newtonian}} \tag{8}$$

These expressions are found to be the Newtonian equations for normal force of a truncated cone multiplied by the factor, q_1/q_∞.

A more general form of equation (8) is obtained if q_1 and θ are treated as functions of r but not of φ, which results in

$$C_{N_{\alpha_1}} = 4 \int_1^{r_b/r_c} \frac{q_1(r)}{q_\infty} \cos^2\theta \, \frac{r}{r_c} \, d\,\frac{r}{r_c} \tag{9}$$

where $q_1(r)$ is the functional dependence of q_1 on r. The variation in dynamic pressure along the flare shock wave is now taken into account, and flare surfaces of curved profile may be included.

The restoring moment due to the flare, about the flare leading-edge station as moment center, is expressible, for an elemental portion of the flare between x and x + dx, as

$$dC_{m_{\alpha_1}} = \left(\frac{X}{r_c}\right) dC_{N_{\alpha_1}} \tag{10}$$
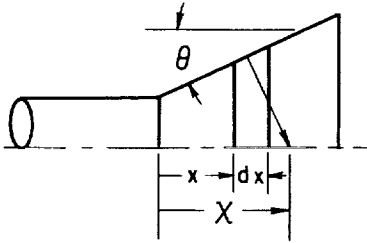
where, as can be seen in the adjoining sketch,[1]

$$X = x + r \tan\theta + \frac{1}{2}(dx + dr \tan\theta) \tag{11}$$

In the limit as dx → 0, this leads to

$$dC_{m_{\alpha_1}} = 4 \frac{q_1(r)}{q_\infty} \cos^2\theta \left(\frac{x}{r_c} + \frac{r}{r_c}\tan\theta\right) \frac{r}{r_c} \, d\,\frac{r}{r_c} \tag{12}$$

which is integrated to obtain

$$C_{m_{\alpha_1}} = 4 \int_1^{r_b/r_c} \frac{q_1(r)}{q_\infty} \frac{x}{r_c} \frac{r}{r_c} \cos^2\theta \, d\,\frac{r}{r_c} + 2 \int_1^{r_b/r_c} \frac{q_1(r)}{q_\infty} \left(\frac{r}{r_c}\right)^2 \sin 2\theta \, d\,\frac{r}{r_c} \tag{13}$$

Here, as in equation (9), q_1 and θ are functions of r but not of φ. For constant q_1 on conical flares, equations (9) and (13) may be reduced to an expression for center of pressure.

[1]For other moment centers, equation (10) becomes

$$dC_{m_{\alpha_1}} = \frac{x_{le} + X}{r_c} dC_{N_{\alpha_1}}$$

where x_{le} is the distance from the moment center to the flare leading edge. On integration, this leads to an additional term on the right-hand side of equation (13), $(x_{le}/r_c)C_{N_{\alpha_1}}$.

$$\frac{x_{cp}}{l_f} = \frac{C_{m\alpha_i}}{C_{N\alpha_i}} \frac{r_c}{l_f} = \frac{2}{3} \frac{\left[\left(\frac{r_b}{r_c}\right)^3 - 1 \right] \left(1 + \tan^2\theta\right)}{\left[\left(\frac{r_b}{r_c}\right)^2 - 1 \right] \left(\frac{r_b}{r_c} - 1\right)} - \frac{1}{\frac{r_b}{r_c} - 1} \qquad (14)$$

This becomes the usual expression for center of pressure of a cone when the cylinder radius r_c is set equal to zero.

CONCLUDING REMARKS

Hypersonic flow fields having secondary shock waves generated by ramps embedded within the main disturbed flow field should, according to present considerations, show some interesting characteristics. For example, pressure coefficients in the embedded flow are speed dependent at hypersonic speeds. Pressures on flares located downstream of a blunt nose are found to be lower than predicted by simple Newtonian theory - in one example, about 1/5 as great. Pressures on ramps located in higher pressure regions of the flow where the Mach number is still supersonic are found to disagree in the opposite sense with Newtonian theory. A flap at the base of a round-nosed cone of 30° half-angle was calculated to have a maximum pressure coefficient of 5 compared to a Newtonian pressure coefficient of 1.5. Pressure coefficients in excess of the maximum possible in Newtonian flow are attributed to a more efficient compression process than a single shock wave process.

These results were obtained by treating the secondary flow over the ramp as an embedded Newtonian impact flow. This concept is valid for thin shock layers when the flow is not extensively separated. Available information on cones and wedges in uniform streams indicates that many cases of practical interest will satisfy the thin-shock-layer requirement. The attached-flow requirement cannot be quantitatively discussed at the present state of knowledge, but it is known that ramps of not too great angle or height relative to other body dimensions will permit attached flow at Reynolds numbers in the order of a few million. In cases where the flow is separated, knowledge of the separated flow geometry may permit application of this concept to the estimation of pressures for these cases also.

Ames Research Center
    National Aeronautics and Space Administration
        Moffett Field, Calif., Feb. 20, 1962

REFERENCES

1. Seiff, Alvin, and Whiting, Ellis E.: The Effect of the Bow Shock Wave on the Stability of Blunt-Nosed Slender Bodies. NASA TM X-377, 1960.

2. Seiff, Alvin, and Whiting, Ellis E.: A Correlation Study of the Bow-Wave Profiles of Blunt Bodies. NASA TN D-1148, 1962.

3. Seiff, Alvin, and Whiting, Ellis E.: Calculation of Flow Fields From Bow-Wave Profiles for the Downstream Region of Blunt-Nosed Circular Cylinders in Axial Hypersonic Flight. NASA TN D-1147, 1961.

4. Maslen, S. H., and Moeckel, W. E.: Inviscid Hypersonic Flow Past Blunt Bodies. Jour. Aero. Sci., vol. 24, no. 9, Sept. 1957, pp. 683-693.

5. Staff of the Computing Section (under the direction of Zdenek Kopal): Tables of Supersonic Flow Around Cones. Tech. Rep. I and III, Center of Analysis, M.I.T., Cambridge, 1947.

6. Feldman, Saul: Hypersonic Gas Dynamic Charts for Equilibrium Air. Avco Res. Lab., Jan. 1957.
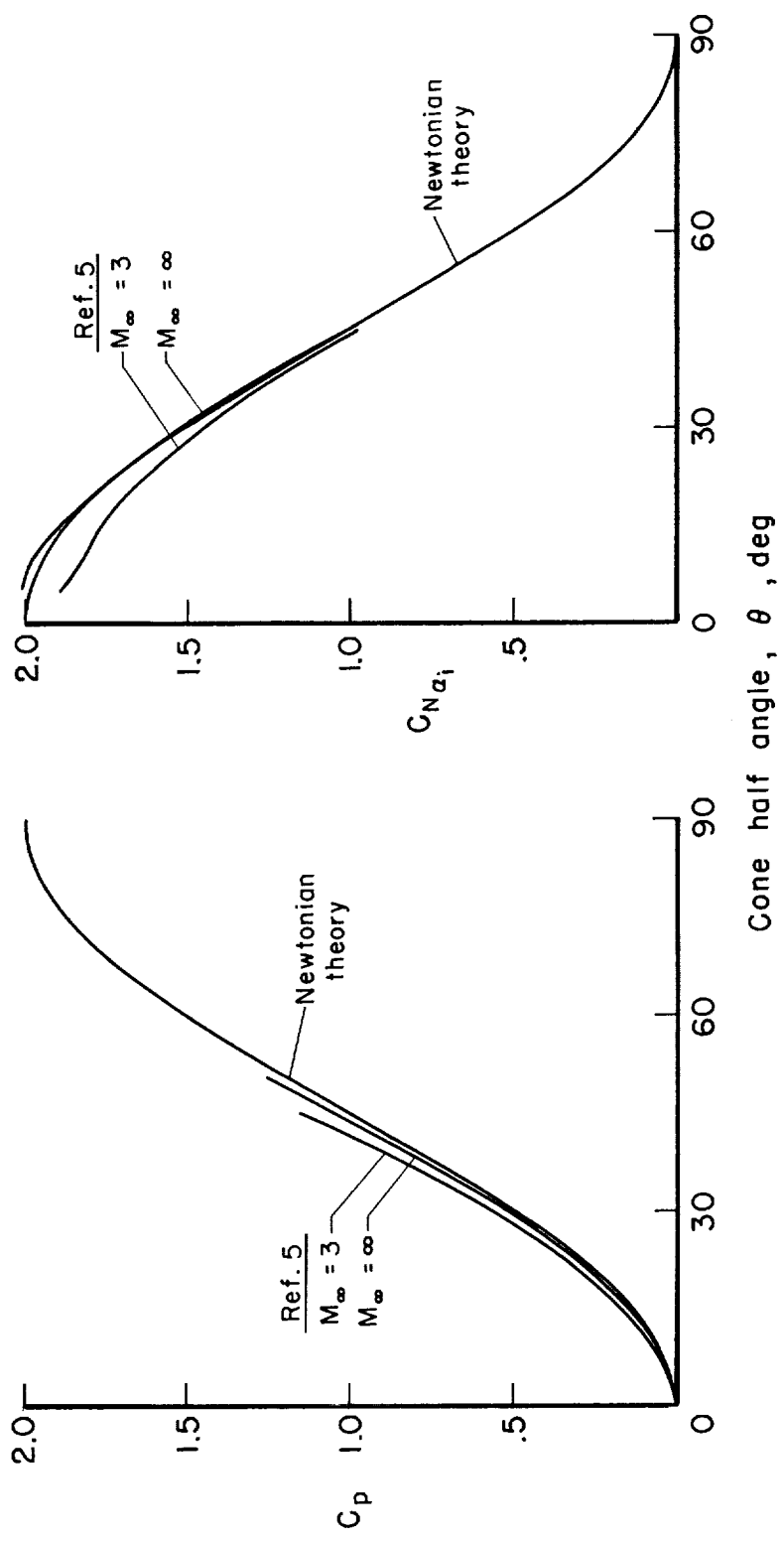
(a) Surface pressure coefficient   (b) Initial normal-force curve slope

Figure 1.- Accuracy of Newtonian theory for pointed cones in a uniform stream.
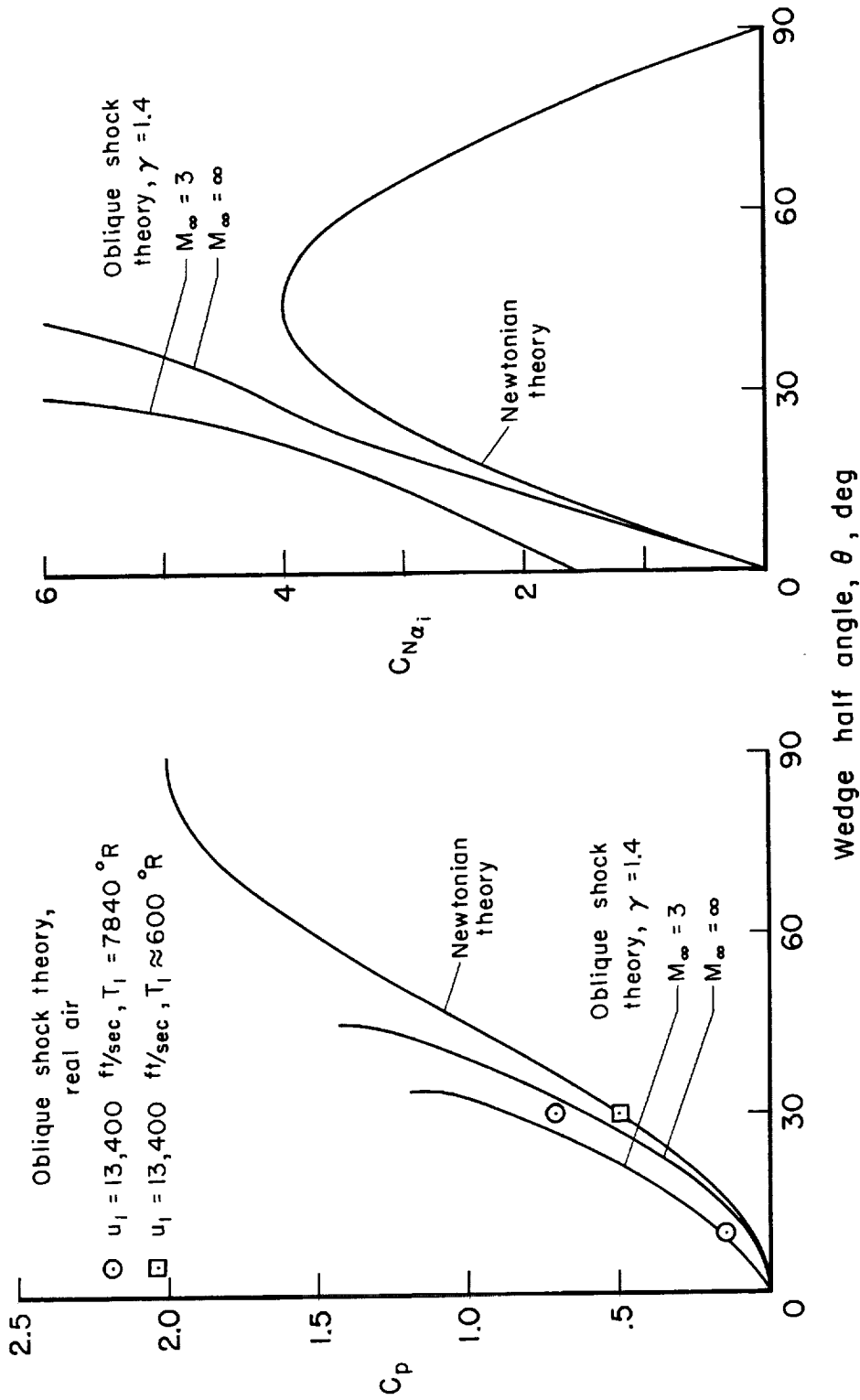
(a) Surface pressure coefficient

(b) Initial normal-force curve slope

Figure 2.- Accuracy of Newtonian theory for two-dimensional wedge flow in a uniform stream.
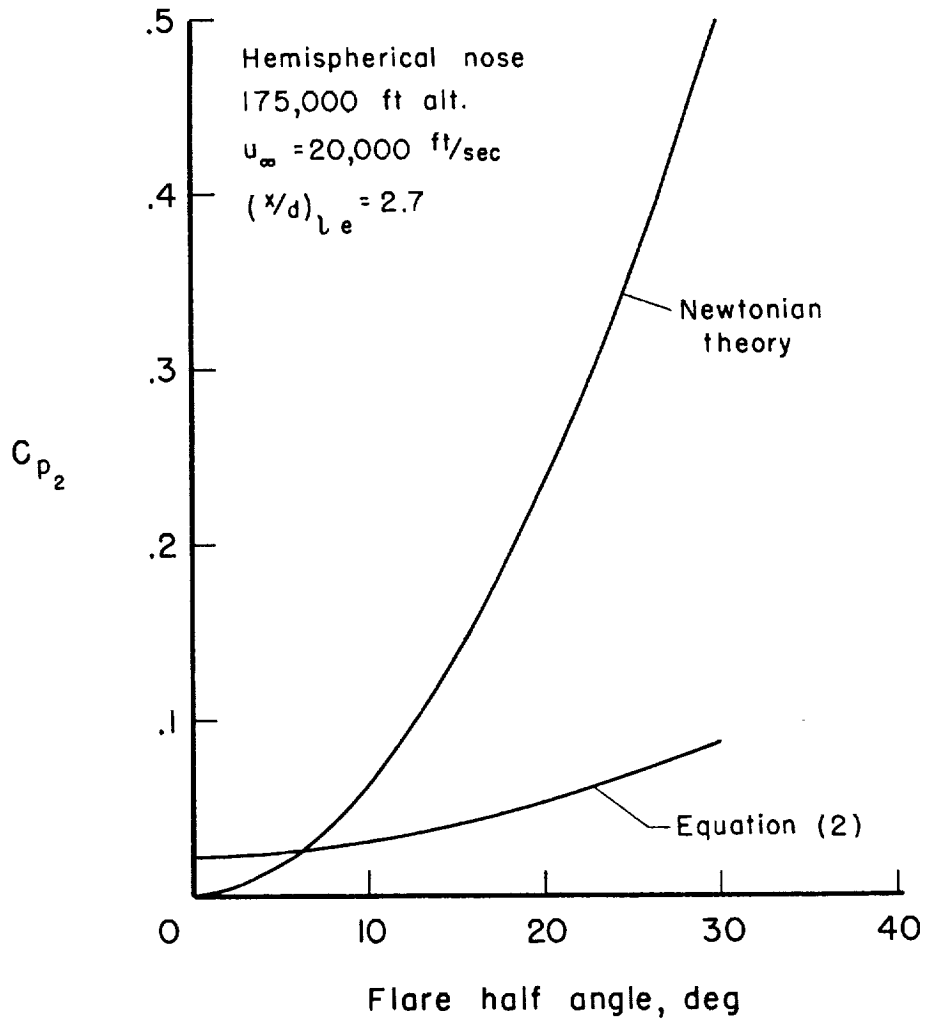
Figure 3.- Comparison of pressures on flares predicted by equation (2) with those given by Newtonian theory.
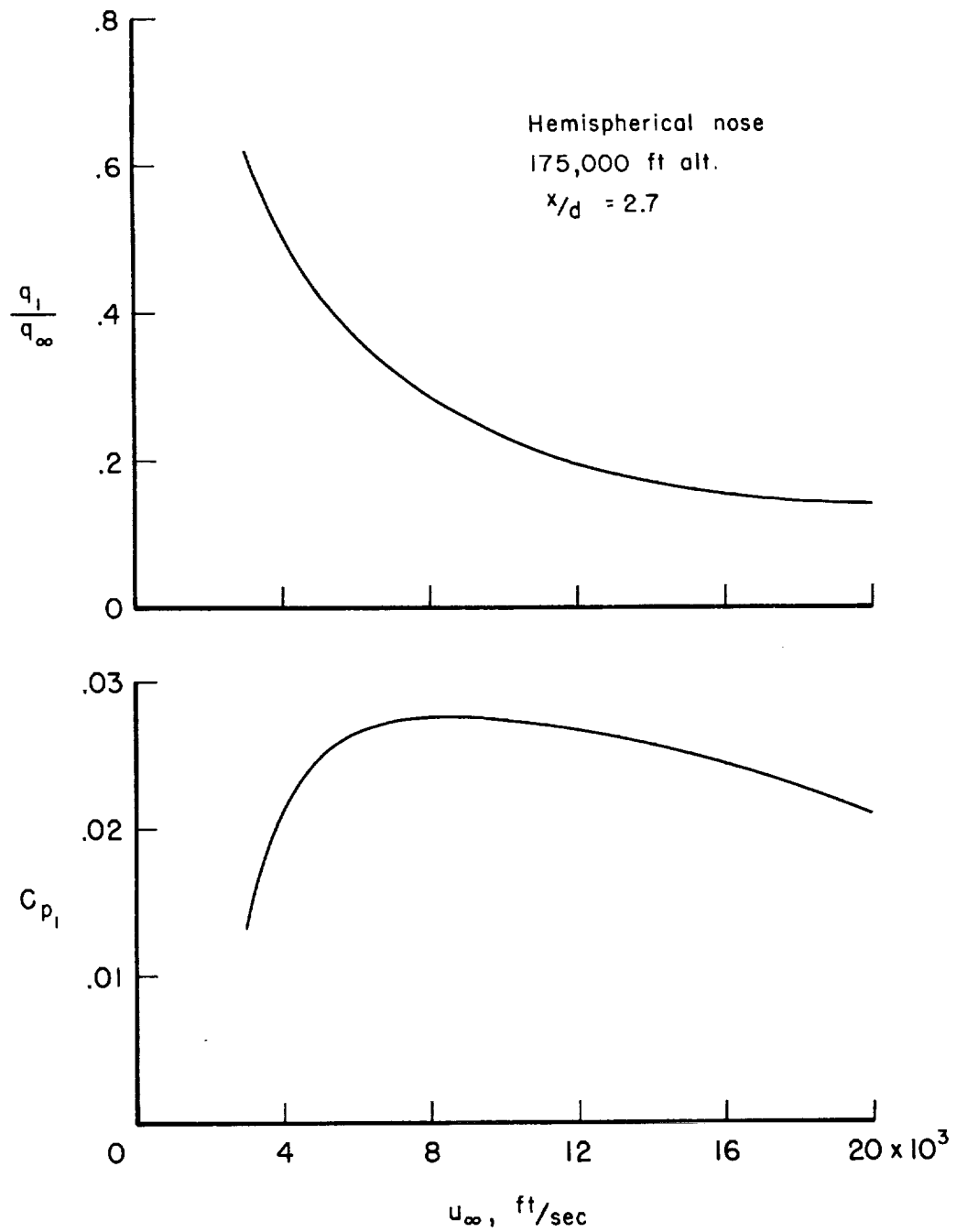
Figure 4.- Variation with speed of conditions at a point on the surface of a hemisphere-cylinder.
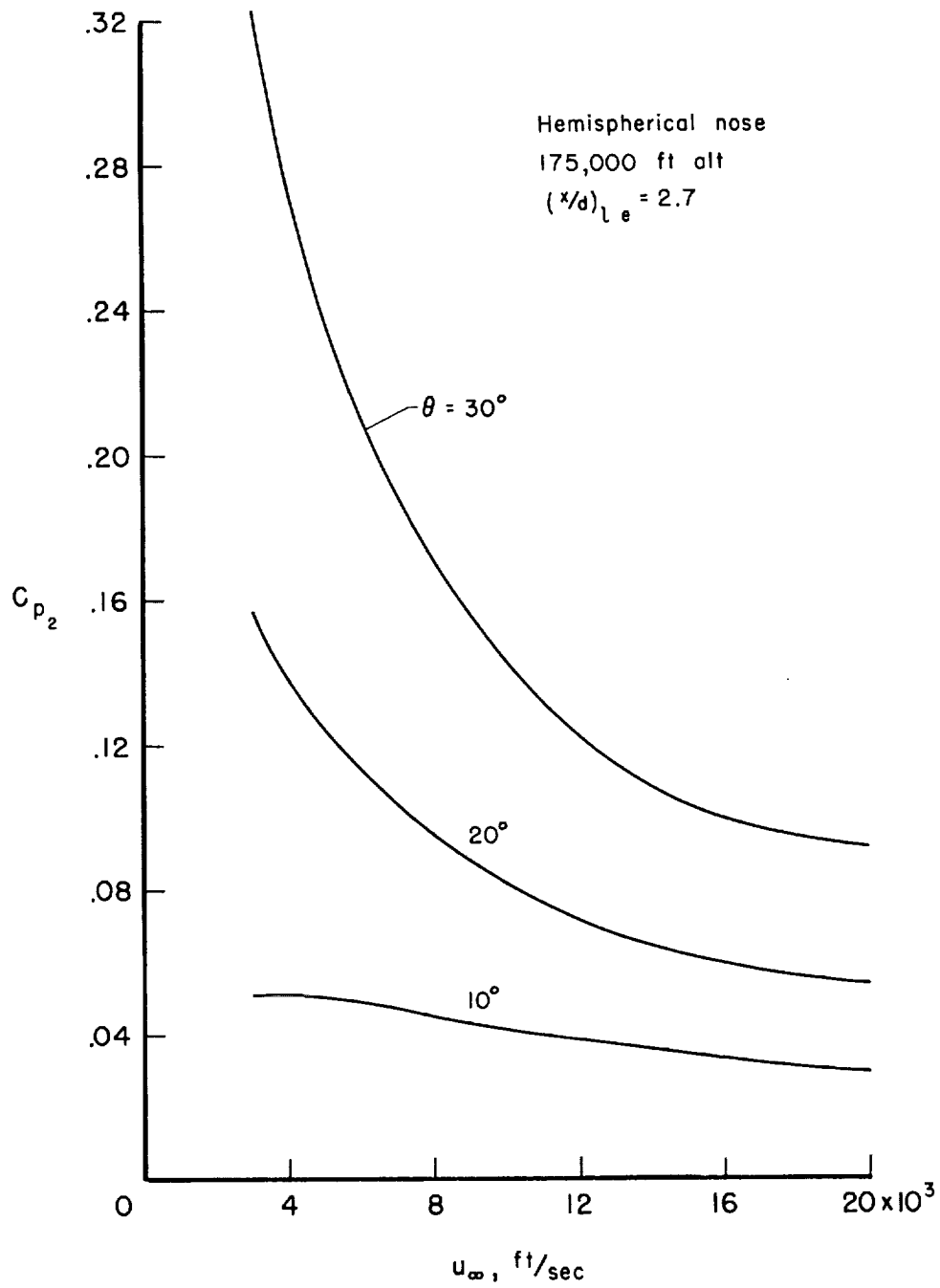
Figure 5.- Predicted variation with flight speed of pressure coefficient at flare leading edge.
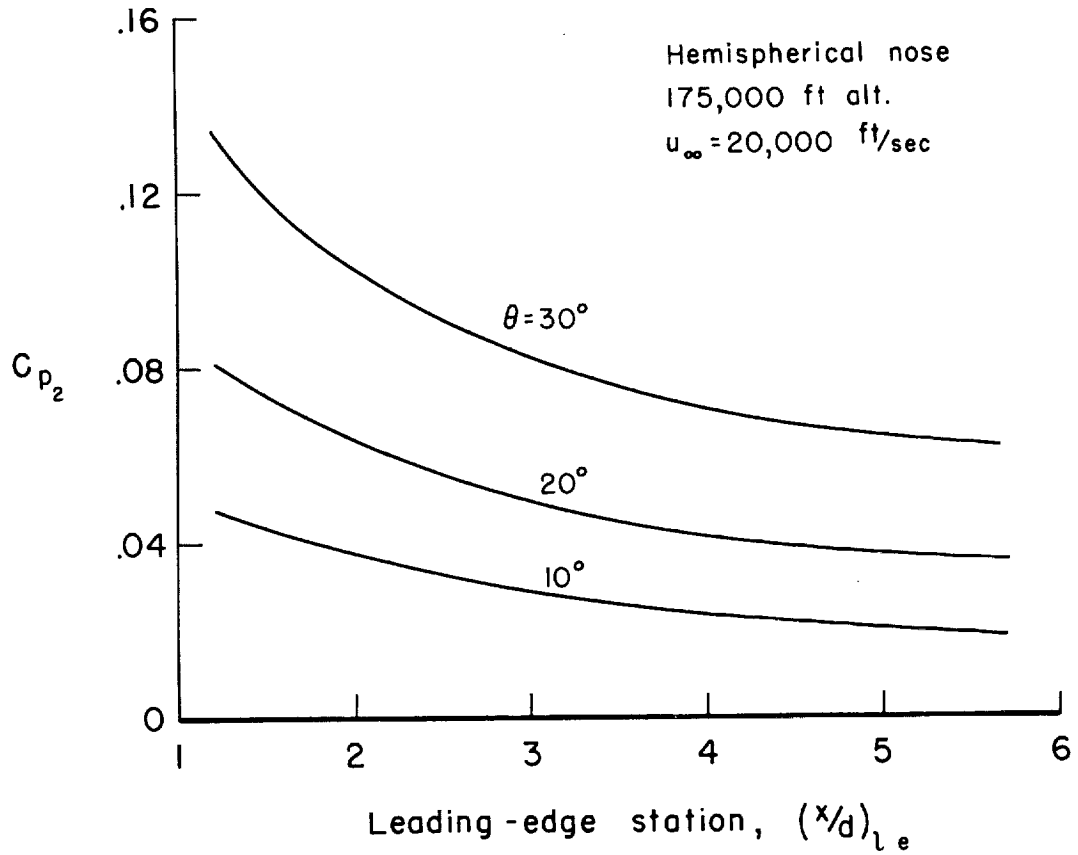
Figure 6.- Predicted variation with leading-edge station of static
pressure at flare leading edge.
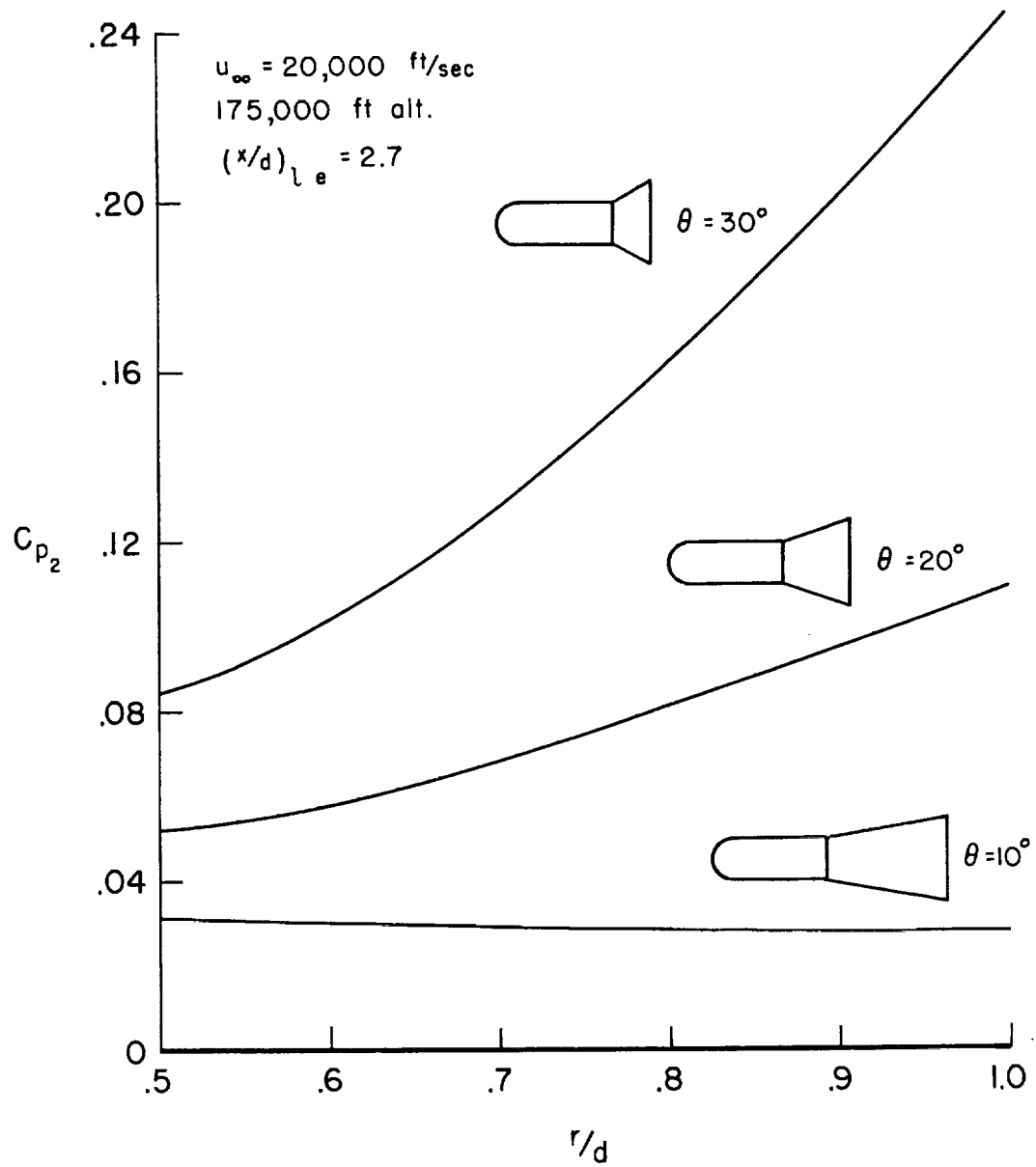
Figure 7.- Predicted variation of static pressure along flare surface.
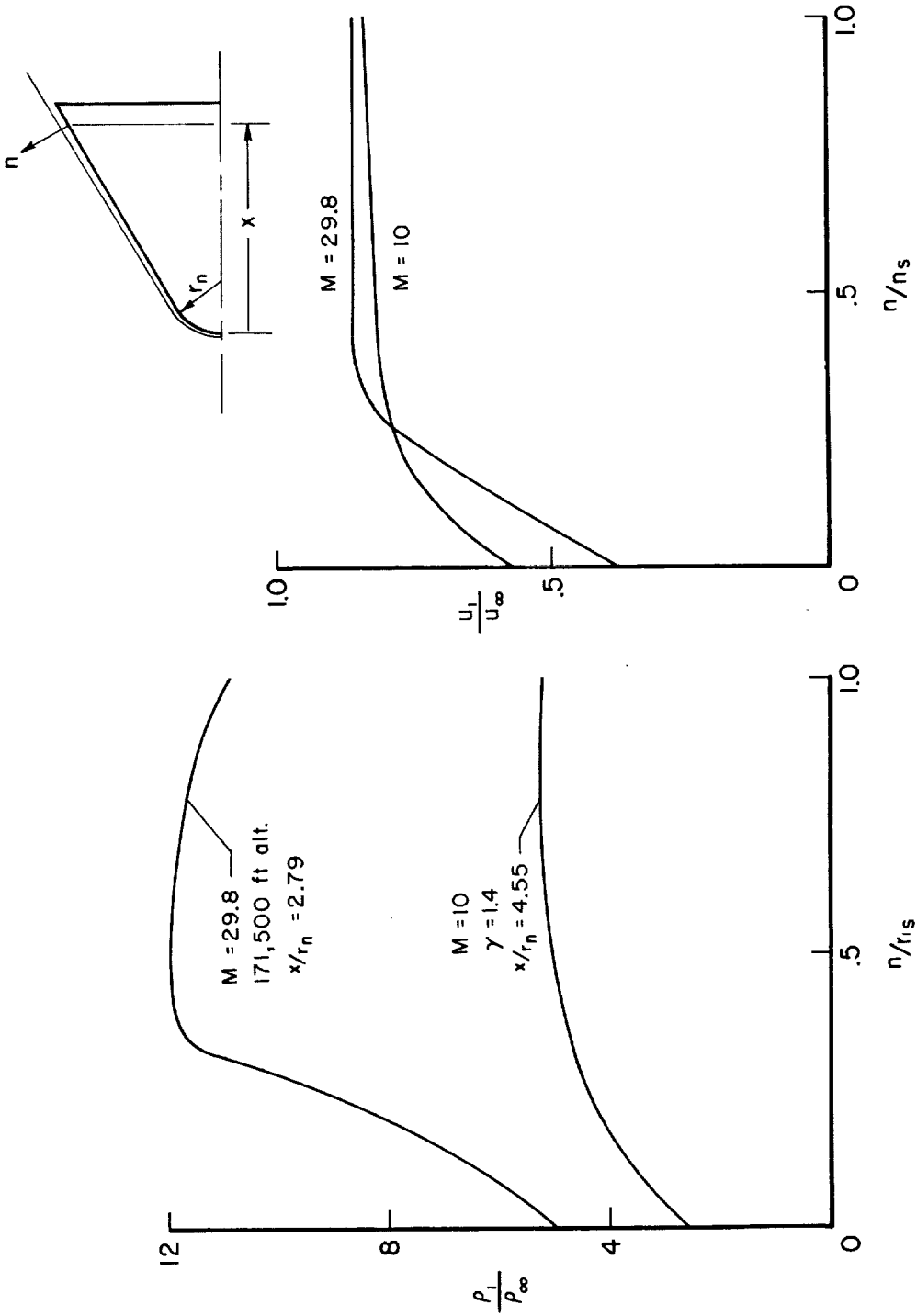
Figure 8.- Density and velocity profiles in shock layer of a 30° round-nosed cone.
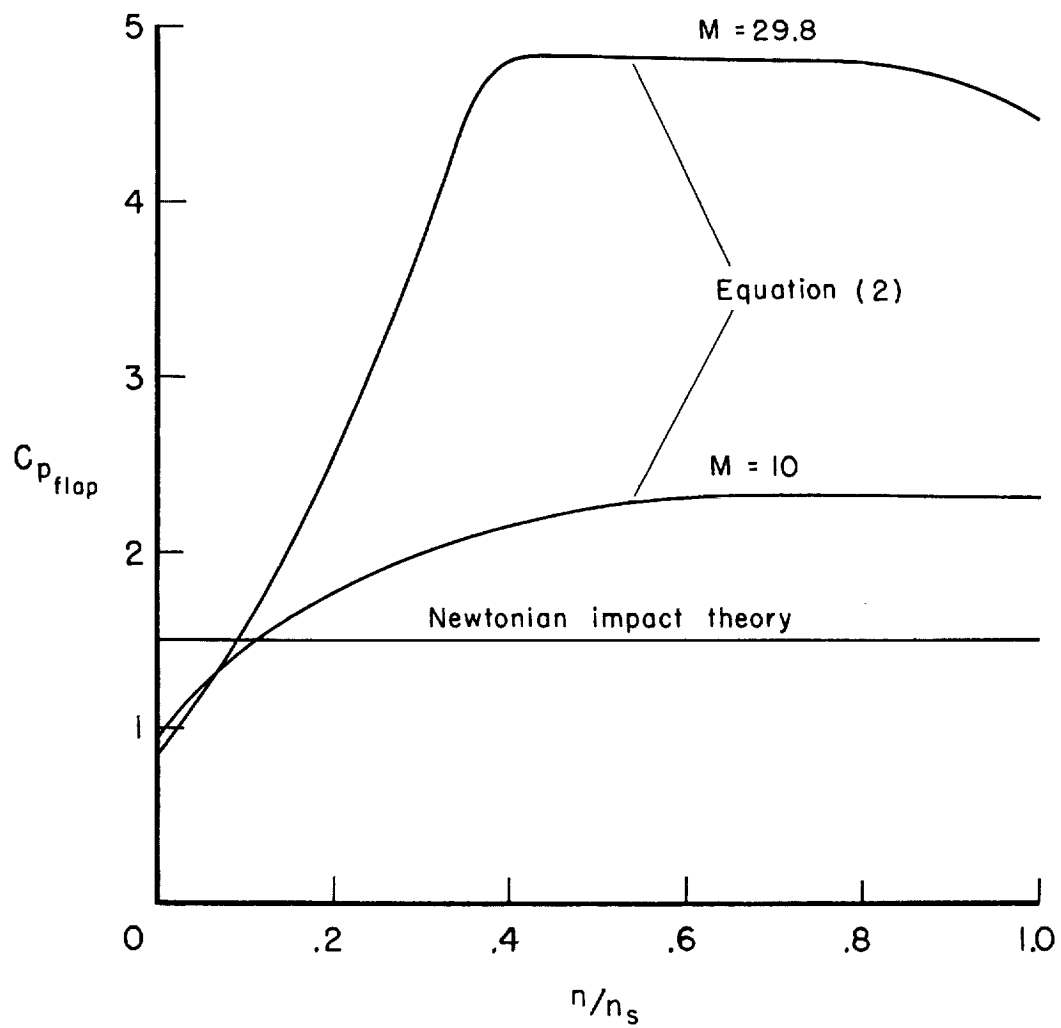
Figure 9.- Flap pressure coefficients predicted by equation (2) for 30° flap deflection.

NASA TN D-1304
National Aeronautics and Space Administration.
SECONDARY FLOW FIELDS EMBEDDED IN HYPER-
SONIC SHOCK LAYERS. Alvin Seiff. May 1962.
23p. OTS price, $0.75.
(NASA TECHNICAL NOTE D-1304)

The flow over ramps, such as flare stabilizers and
control flaps, which are located in supersonic regions
behind the bow shock wave on bodies in hypersonic
flight, is examined. An embedded Newtonian impact
flow concept is proposed. The appropriateness of
this concept is discussed. A simple pressure
equation is derived which requires knowledge of the
characteristics of the local stream incident on the
ramp shock wave. Pressures on embedded ramps
are found in examples to differ from those predicted
by usual Newtonian theory, by factors varying from
1/5 to 3. Dependence of the pressure coefficients
on speed in the hypersonic range is predicted.
Equations for the initial slopes of normal-force and

Copies obtainable from NASA, Washington

NASA

I.   Seiff, Alvin
II. NASA TN D-1304

(Initial NASA distribution:
2, Aerodynamics, missiles
and space vehicles;
20, Fluid mechanics;
50, Stability and control.)

NASA TN D-1304
National Aeronautics and Space Administration.
SECONDARY FLOW FIELDS EMBEDDED IN HYPER-
SONIC SHOCK LAYERS. Alvin Seiff. May 1962.
23p. OTS price, $0.75.
(NASA TECHNICAL NOTE D-1304)

The flow over ramps, such as flare stabilizers and
control flaps, which are located in supersonic regions
behind the bow shock wave on bodies in hypersonic
flight, is examined. An embedded Newtonian impact
flow concept is proposed. The appropriateness of
this concept is discussed. A simple pressure
equation is derived which requires knowledge of the
characteristics of the local stream incident on the
ram) shock wave. Pressures on embedded ramps
are found in examples to differ from those predicted
by usual Newtonian theory, by factors varying from
1/5 to 3. Dependence of the pressure coefficients
on speed in the hypersonic range is predicted.
Equations for the initial slopes of normal-force and

Copies obtainable from NASA, Washington

NASA

I.   Seiff, Alvin
II. NASA TN D-1304

(Initial NASA distribution:
2, Aerodynamics, missiles
and space vehicles;
20, Fluid mechanics;
50, Stability and control.)

NASA TN D-1304
National Aeronautics and Space Administration.
SECONDARY FLOW FIELDS EMBEDDED IN HYPER-
SONIC SHOCK LAYERS. Alvin Seiff. May 1962.
23p. OTS price, $0.75.
(NASA TECHNICAL NOTE D-1304)

The flow over ramps, such as flare stabilizers and
control flaps, which are located in supersonic regions
behind the bow shock wave on bodies in hypersonic
flight, is examined. An embedded Newtonian impact
flow concept is proposed. The appropriateness of
this concept is discussed. A simple pressure
equation is derived which requires knowledge of the
characteristics of the local stream incident on the
ramp shock wave. Pressures on embedded ramps
are found in examples to differ from those predicted
by usual Newtonian theory, by factors varying from
1/5 to 3. Dependence of the pressure coefficients
on speed in the hypersonic range is predicted.
Equations for the initial slopes of normal-force and

Copies obtainable from NASA, Washington

NASA

I.   Seiff, Alvin
II. NASA TN D-1304

(Initial NASA distribution:
2, Aerodynamics, missiles
and space vehicles;
20, Fluid mechanics;
50, Stability and control.)

NASA TN D-1304
National Aeronautics and Space Administration.
SECONDARY FLOW FIELDS EMBEDDED IN HYPER-
SONIC SHOCK LAYERS. Alvin Seiff. May 1962.
23p. OTS price, $0.75.
(NASA TECHNICAL NOTE D-1304)

The flow over ramps, such as flare stabilizers and
control flaps, which are located in supersonic regions
behind the bow shock wave on bodies in hypersonic
flight, is examined. An embedded Newtonian impact
flow concept is proposed. The appropriateness of
this concept is discussed. A simple pressure
equation is derived which requires knowledge of the
characteristics of the local stream incident on the
ramp shock wave. Pressures on embedded ramps
are found in examples to differ from those predicted
by usual Newtonian theory, by factors varying from
1/5 to 3. Dependence of the pressure coefficients
on speed in the hypersonic range is predicted.
Equations for the initial slopes of normal-force and

Copies obtainable from NASA, Washington

NASA

I.   Seiff, Alvin
II. NASA TN D-1304

(Initial NASA distribution:
2, Aerodynamics, missiles
and space vehicles;
20, Fluid mechanics;
50, Stability and control.)

NASA TN D-1304

pitching-moment curves of flare stabilizers operating in the wake of blunt noses are developed.

Copies obtainable from NASA, Washington

NASA

NASA TN D-1304

pitching-moment curves of flare stabilizers operating in the wake of blunt noses are developed.

Copies obtainable from NASA, Washington

NASA

NASA TN D-1304

pitching-moment curves of flare stabilizers operating in the wake of blunt noses are developed.

Copies obtainable from NASA, Washington

NASA

NASA TN D-1304

pitching-moment curves of flare stabilizers operating in the wake of blunt noses are developed.

Copies obtainable from NASA, Washington

NASA